Mining, Metallurgy & Exploration (2022) 39:2247–2256
https://doi.org/10.1007/s42461-022-00657-2

Real-time Photoacoustic Measurements of the Mass Concentration of Respirable Crystal Silica Dust: Theory

Samuel J. Taylor[1] · Pedro Nascimento[2] · W. Patrick Arnott[1] · Charles Kocsis[3]

Received: 10 March 2021 / Accepted: 6 July 2022 / Published online: 31 July 2022

Abstract
Respirable crystalline silica (RCS) is an inhalation health hazard for mining and industrial work environments and must be monitored. We provide theoretical analysis of real-time measurements for determining RCS mass concentration without the use of filters by using photoacoustic spectroscopy. The suspended dust in the mine air can be continuously sampled by the photoacoustic instrument. A tunable quantum cascade laser is the light source, allowing for determination of interferences such as kaolinite, coal dust, and water vapor. The most useful spectral region is found to be between 11 and 13 μm. Absorption by water vapor, and, to a lesser extent, carbon dioxide, in this spectral region has gaps that allow for quantification of the aforementioned dust species as well as a convenient check on the calibration of the instrument. This work brings photoacoustic measurement of aerosol to the mid infrared range where spectrally dependent light absorption can be used to quantify dust composition and mass concentration.

Keywords Photoacoustic · Real time · Quantum cascade laser · Silica dust · Coal dust · Air quality

1 Introduction

1.1 Nature of the respirable crystalline silica (RCS) health hazard in mining and industry

Coal mining is a substantial industry employing many workers around the world. Due to the nature of the industry, coal miners are frequently exposed to elevated concentrations of airborne RCS. The medical conditions associated with overexposure to airborne silica and coal dust include pneumoconiosis, emphysema, silicosis, and chronic obstructive pulmonary disease, all of which are known to contribute to coal worker's pneumoconiosis (CWP) and other chronic lung diseases [1]. This respirable health hazard can have a truly overwhelming effect upon the life of a coal worker, sometimes leading even to premature death. Respirable [2] coal mine dust consists of airborne particles of coal, silica, other minerals, and various types of organic material generated by mining activities. These particles can be inhaled into the deepest parts of the lung, damaging lung function by embedding into and destroying alveoli, a critical structure allowing the transfer of oxygen into the bloodstream [3]. This can have a very harmful and long-lasting effect on the lungs because the body has very few means of removing hazardous material of this size from this region. Data collected by NIOSH shows that the prevalence rate of lung disease among US coal miners continues to be a problem [4]. The effects of silicosis and other forms of chronic lung disease brought on by exposure to RCS are felt in many other fields as well [5]. Therefore, it is important to monitor RCS concentrations in order to prevent the exposure of workers to high concentrations and to avoid future health problems.

1.2 Discussion of the Current Monitoring Techniques

Currently, there are three primary methods for monitoring silica and coal dust: (1) NIOSH 7500, 7601, and 7603 laboratory methods after samples are collected on filter media, (2) personal dust monitoring that provides total dust concentration readings in a near-continuous manner, and (3)

✉ W. Patrick Arnott
arnottw@unr.edu

[1] Department of Physics, Atmospheric Science Program, University of Nevada, Reno, Reno, NV, USA

[2] Department of Mining and Metallurgical Engineering, University of Nevada, Reno, Reno, NV, USA

[3] Department of Mining Engineering, The University of Utah, Salt Lake City, UT, USA

a field-based method using an on-site Fourier transform infrared spectrometer (FTIR) for analyzing filters collected during a workshift.

The most well-known method for monitoring RCS in mining environments comprise the NIOSH 7500, 7601, and 7603 techniques. These techniques involve the offsite preparation of samples via ashing or dissolution of the filter to remove interfering materials, followed by redeposition onto a new filter [6]. Due to the shipping, preparation, and calculation time needed for these methods, it often takes anywhere from 1 to 2 weeks for the dust concentration results to be posted to the mine site. This comes with the obvious drawback of severe lag time between exposure to potentially hazardous levels of RCS and alerting the exposed individuals. Additionally, because the techniques are filter-based methods, the measurement time typically occurs over the course of about 8 h. In this case, all that can be known is the time-weighted average RCS concentration [6]. So, while effective at determining RCS concentrations over the sampling period, this method has the drawback of being slow. In addition, due to time-weighted average concentration measurements, the short-term, elevated dust concentrations in the production areas and throughout the mine cannot be identified.

The continuous personal dust monitor (CPDM), namely the PDM3700 sold by Thermo-Scientific, is an instrument that provides 30-min averages of total respirable aerosol mass concentrations. The PDM3700 uses a tapered element oscillating microbalance to measure the concentration of airborne particulate matter [3]. Coupling this device with a cyclone designed to sort particles into the desired size ranges allows for accurate measurement of respirable aerosol mass concentration. The device cannot discern between coal dust, silica dust, and other types of material present in the atmosphere and instead only gives a concentration of the total airborne particulate matter [7].

Recently, NIOSH has developed a field-based method for measuring respirable silica concentrations to reduce the 1 to 2 weeks wait time for dust concentration data. While it is not a real-time method, it provides a way to determine RCS concentrations at mine sites immediately after the end of a work shift. An air sampling system made up of a personal sampling pump, a respirable aerosol cyclone, and dust sampling cassette is used to collect airborne dust onto a filter throughout a miner's shift. Once the miner's shift has ended, the sampled filter is removed for analysis. An onsite Fourier transform infrared spectrometer (FTIR) capable of evaluating the filter sample absorbance over a spectral range of 4000–400 cm^{-1} with a resolution of 4 cm^{-1} is required [7]. NIOSH has created and made public their software known as the NIOSH Field Analysis of Silica Tool for determining the mass concentration of RCS [7].

The need for a real-time instrument to accurately measure RCS is critical. The measurement method and instrument discussed below is capable of determining airborne silica mass concentrations in real time without the need for deposition on a filter. The following discussion provides the theoretical foundation for this method and the wavelengths used for analysis.

2 Optical Measurements of Respirable Crystalline Silica Mass Concentration

2.1 Real-Time Measurements of Aerosol Light Absorption

A review of the relevant terminology and concepts underlying the method provides a framework for the discussion in this manuscript. Figure 1 illustrates the basic interactions of light and dust aerosol.

Light is incident on a plume of dust aerosol, and portions of the light are scattered, absorbed, and transmitted to the detector [8]. Absorbed light heats the aerosol, while scattered light is available for further interactions with the dust plume. These aerosol optical properties depend on aerosol size, composition, morphology, and mixing state [8]. The most important observation for the current work is that

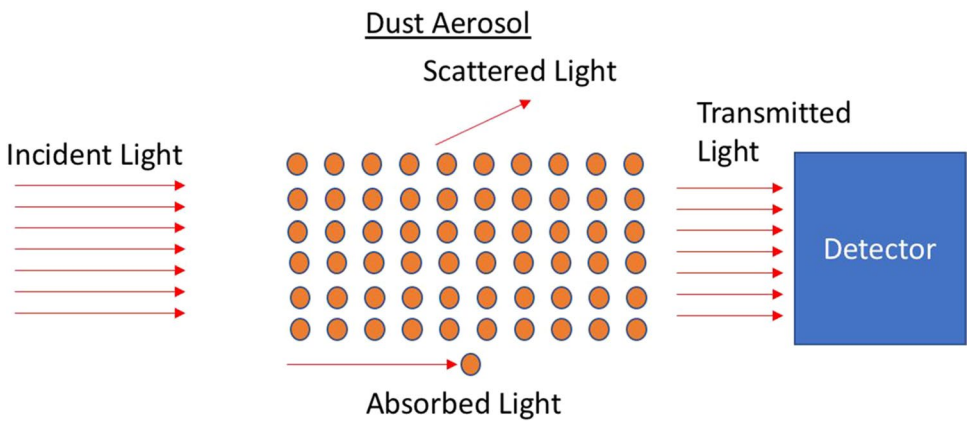

Fig. 1 Interaction of light and dust aerosol, possibly a complex mixture of coal, SiO_2, and kaolinite. In practice, the dust is not arranged in a regular array as shown here but is randomly distributed

when aerosol light absorption occurs throughout the entire aerosol volume, it is proportional to aerosol mass concentration needed for health applications, as discussed below. The photoacoustic instrument described below [9] directly measures aerosol light absorption by freely suspended aerosol (no filters are used) and the transmitted light measured with the detector shown in Fig. 1 can be used to calibrate these measurements [10]. The NIOSH spectroscopic filter-based method used for end-of-shift detection of silicate dust aerosol deposited on filters involves the additional interaction of a light-aerosol-filter-detector and makes use of a Fourier transform infrared spectrometer for performing the functions of light source and detection [11]. The discussion in Sec. 2b applies to both the photoacoustic method and the NIOSH methods for RCS quantification since they both involve measurements of the optical properties of aerosol.

An ideal detector of RCS in the presence of coal and other mineral dust like kaolinite would consist of an absorption measurement with a laser of wavelength such that it is strongly absorbed by RCS and is negligibly absorbed by the other species present. Additionally, the light absorption would occur throughout the entire volume of RCS aerosol so that the absorption measurement would be sensitive to the total mass of SiO_2 per unit volume in the dust sample as is the current practice used in RCS health related measurements.

Figure 2 shows the schematic of a photoacoustic instrument [12]. Sample air enters the instrument on the left, is pulled through the acoustical resonator in the center region, and exits on the right. A power modulated quantum cascade laser beam (QCL) enters on the left and exits on the right to a laser power meter. The modulation frequency of the QCL is set to match the acoustical resonator frequency. RCS present in the center region will absorb laser light and heat. The heat is then transferred to the surrounding air, resulting in thermal expansion. A micro speaker (not shown) is used to calibrate the acoustical resonator to make sure the proper frequency is maintained. The quantum cascade laser wavelength can be tunable to cover a range of wavelengths for quantifying RCS, kaolinite, and coal dust [13].

The photoacoustic instrument operation is summarized as follows [14]. First, the laser light is power modulated with a square wave. Light absorbing aerosols convert the light into heat that is transferred to the surrounding air, and acoustic pressure is created in the resonator. A standing wave of sound having the modal shape labeled "Acoustic Mode" in Fig. 2 is produced because the laser is modulated at the resonance frequency. The microphone measures the sound at the frequency of the laser power modulation. Finally, the sound signal corresponds to the aerosol light absorption and silica dust mass concentration with a proper choice of laser wavelength that is absorbed by silica. The acoustical resonator is in the center section. The resonance frequency of this instrument is nominally 1500 Hz as a compromise between instrument size and thermal response time of the aerosol. "Noise Filters" are volumes tuned by adjusting their length to reflect noise at the operating frequency coming in from the sample inlet and outlet to avoid sound interference to the sensitive microphone within the resonator.

The measurement of light absorption by silica dust can be achieved by using the photoacoustic equation to relate the sound pressure and laser power to the aerosol light absorption coefficient β_{abs} [14],

$$\beta_{\text{abs}} = \frac{P_{\text{m}}}{P_{\text{L}}} \frac{A_{\text{res}}}{\gamma - 1} \frac{\pi^2 f_0}{Q} \tag{1}$$

where P_{m} and P_{L} are the microphone pressure and laser power at the resonant frequency f_0 determined with the speaker and microphone; A_{res} is the cross-sectional area of the resonator; $\gamma = 1.4$ is the ratio of isobaric and isochoric specific heats for air; and Q is the quality factor of the resonator. A calibrated microphone and laser power meter are used so that accurate values are entered in Eq. (1). The accuracy of Eq. (1) has been tested by calibration of instruments using light absorbing gases [15]. The aerosol light absorption coefficient is the quantity which is also measured in the

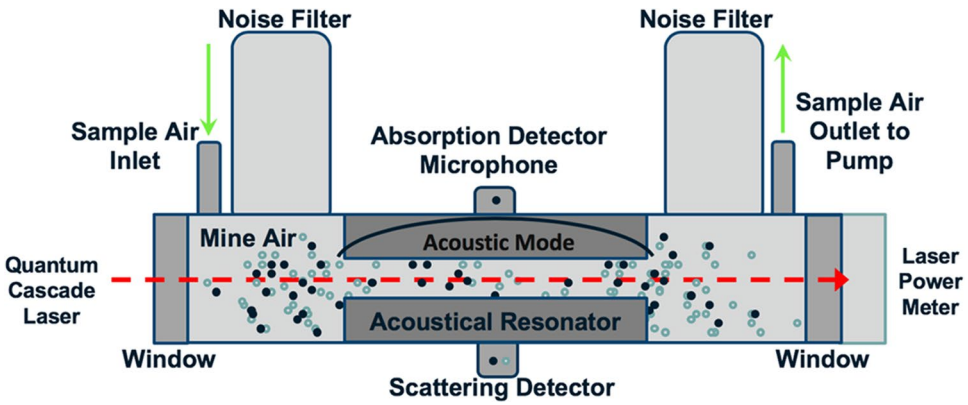

Fig. 2 Schematic of the photoacoustic instrument. The half wavelength acoustic resonator is in the center of the instrument. The acoustic mode indicates a pressure antinode at the resonator center and nodes just outside the resonator on each side. The instrument measures both light scattering and absorption. For illustration purposes, aerosol diameter is greatly exaggerated, and concentration is typically much greater than shown in this schematic

filter-based FTIR measurements of RCS [11, 13]. Aerosol light absorption at UV, visible, and near IR wavelengths is also used to measure black carbon mass concentration by photoacoustic and filter-based techniques [16]. Once the aerosol light absorption coefficient is measured, the mass concentration of silica dust is obtained as presented in Sect. 2.b.

Having discussed photoacoustic measurement of aerosol light absorption, a partial history of the method is given here to place the current effort in context. Early instruments were trailer size due to the use of large gas lasers as the light source [17]. Use of solid state lasers greatly reduced instrument size and complexity because the lasers are much smaller, require much less power, and can be electronically modulated rather than modulation with a mechanical chopper [14]. The use of 1047-nm laser wavelength has been demonstrated for measurement of black carbon aerosol emitted by vehicles being tested on dynamometers [18]. These instruments are robust enough to be used on meteorological aircraft to measure aerosol light absorption and scattering aloft [19]. A compact, portable microcontroller-based instrument using a 660-nm laser diode was recently demonstrated in the laboratory for measurements of aerosol light absorption by coal dust and aerosol light scattering by coal and silica dust [12]. Our current work brings photoacoustic measurement of aerosol to the mid infrared range where spectrally dependent light absorption can be used to quantify dust composition. The ultimate goal is to develop a personal sampler for dust composition measurement using compact photoacoustic instruments equipped with tunable quantum cascade lasers.

2.2 Theory of Light Absorption by RCS and Kaolinite

2.2.1 Refractive Indices of Alpha Quartz and Kaolinite and Other Minerals

The complex refractive index, m, is a material property that determines the interaction of light with matter [8]. The notation used is

$$m = n + ik \tag{2}$$

where n and k are the real and imaginary parts. Light absorption is primarily associated with the imaginary part. Figure 3 shows the complex refractive index for many minerals likely to be found suspended in the atmosphere, both as internally mixed combinations and as an externally mixed single composition aerosol. For example, alpha quartz (gray curves) has a relative maxima imaginary part at around 9.2 μm and 12.44 μm due to the resonant interaction of light at these wavelengths with quantum mechanical modes of vibration, and it is larger than other minerals. The most common mineral interferent for RCS determination is kaolinite [11], though the spectra in Fig. 3 are useful for understanding interference by other minerals. The complex refractive indices of dust are needed to model the infrared radiative impacts of these aerosol [20].

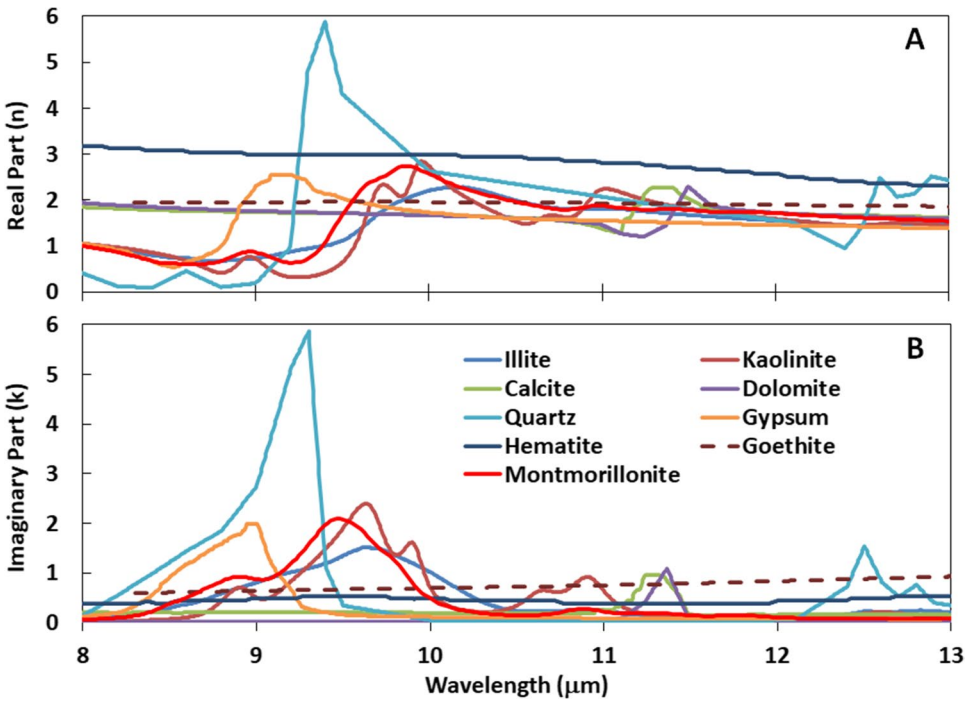

Fig. 3 Complex refractive indices for various minerals, adapted from [20]

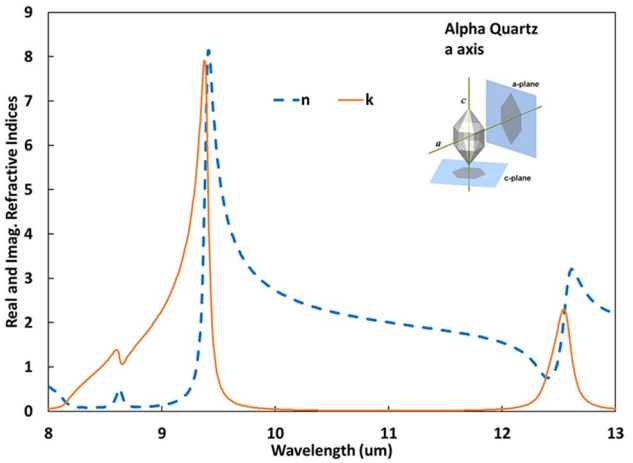

Fig. 4 Real and imaginary parts of the refractive indices of alpha quartz for incident light with polarization parallel to the a-axis, from [21]. Inset crystal figure is from http://www.quartzpage.de/gen_struct.html

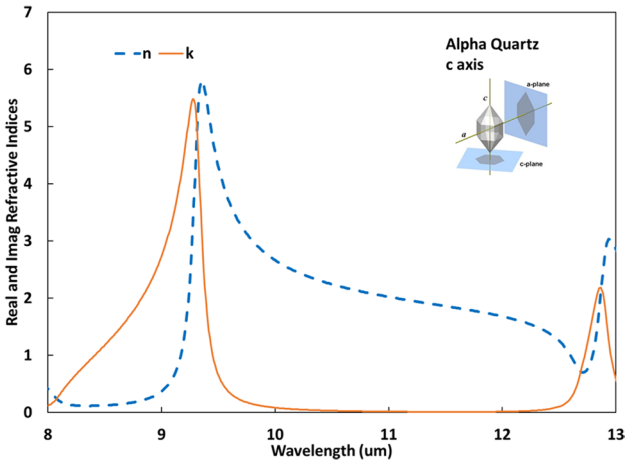

Fig. 5 Same as Fig. 4 but for the c-axis, from [21]. Inset crystal figure is from http://www.quartzpage.de/gen_struct.html

Alpha quartz, as a birefringent crystal, has different refractive indices for light with polarization parallel to the "a" (Fig. 4) and "c" (Fig. 5) crystallographic axes. The wavelength range 8–13 μm is where the atmosphere is relatively transparent so that aerosol absorption can be measured without much gaseous absorption interference. The complex refractive indices of kaolinite is shown in Fig. 6. The real and imaginary parts of the complex refractive index, along with aerosol size and morphology, are used to determine the amount of light absorption and scattering by these particles. Spherical particles of diameter D are assumed. The relationships among aerosol diameter, wavelength of the light source, and complex refractive index will be used to choose a laser wavelength for measuring the mass concentration of SiO_2 dust.

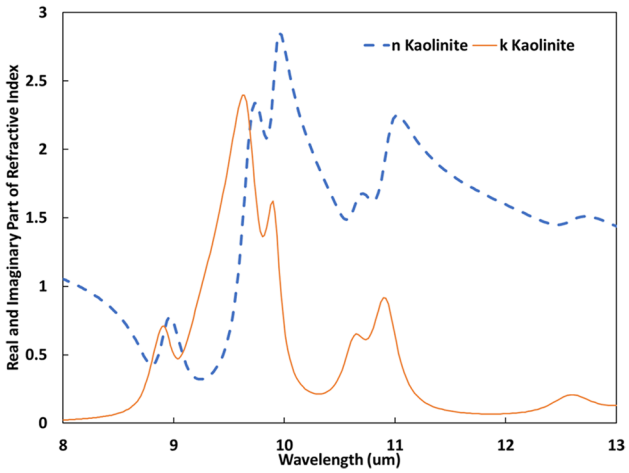

Fig. 6 Same as Fig. 4 but for kaolinite [22]

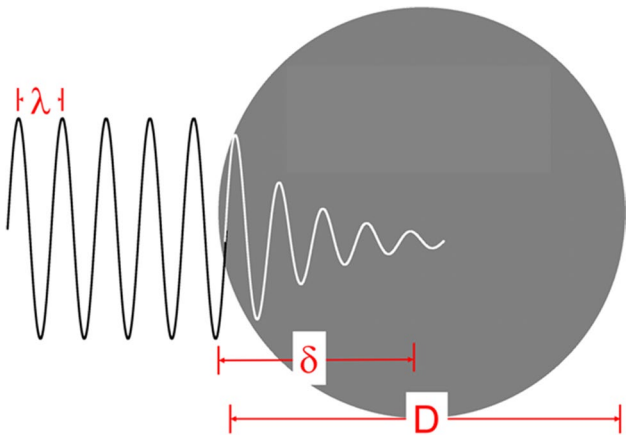

Fig. 7 Schematic showing light penetration depth δ into a spherical particle of diameter D

2.2.2 Light Penetration Depth in SiO_2 and Kaolinite Aerosol

The light penetration depth, δ, into an aerosol particle is given by [8]

$$\delta = \frac{\lambda}{4\pi k} \tag{3}$$

where λ is the light wavelength, and k is the imaginary part of the refractive index from Eq. (2). This parameter provides a semi-quantitative understanding of the interaction of radiation at various wavelengths with dust aerosol. Figure 7 is a schematic of the light penetration depth of a spherical particle.

Three regimes are identified:

- $\delta << D$ Light is absorbed mostly by the surface of the particle, ideal for surface area measurements.

- $\delta \approx D$ Light is absorbed within the aerosol diameter (resonance regime).
- $\delta >> D$ Light is absorbed throughout the entire particle volume, ideal for measuring the mass concentration of the aerosol. However, absorption strength is smaller in this regime.

Large values of the imaginary part of the refractive index result in small light penetration depths. For example, in Fig. 5, 9.2 microns corresponds to a peak in the imaginary part of the refractive index. Often, a compromise must be made so that light absorption by the desired species (SiO_2) is strong enough to occur over the entire particle volume for mass concentration measurement but is weak for interfering species such as kaolinite. Figure 8 shows the light penetration depth for SiO_2 and kaolinite. The absorption band around 8.5 µm for SiO_2 is associated with a penetration depth less than a micron and is different from that of kaolinite. At 12.8 µm, the light penetration depth for SiO_2 is much greater.

2.2.3 Small Particle Limit for Light Absorption by SiO_2 and Kaolinite

The small particle limit for light absorption is based on an analytical solution of the theory for spheres, taking into account only the first term [8]. It is accurate when the aerosol diameter is much smaller than the light penetration depth. The most useful parameter is the mass absorption efficiency, *MAE*, which is also known as the aerosol absorption cross section per aerosol mass, commonly expressed in units of [m^2/gram]. It is given by:

$$MAE = \frac{6\pi}{\rho_p \lambda} IM\left\{\frac{m^2-1}{m^2+2}\right\} \tag{4}$$

where ρ_p is the aerosol density (2.65 g cm^{-3} for SiO_2 and 2.61 g cm^{-3} for kaolinite); m is the complex refractive index of Eq. (2); and the IM selects the imaginary part of the quantity in the brackets. Equation (4) depends both on the real and imaginary parts of the refractive index. Especially notice that *MAE* is independent of aerosol diameter; therefore, in this limit the *MAE,* typically given in units of m^2/gram, depends only on the aerosol mass. In this limit, light absorption measurements by photoacoustic instruments and Fourier transform infrared spectrometers can be expressed as:

$$\beta_{\text{abs}} = MAE\rho \tag{5}$$

where β_{abs} is the absorption coefficient, and ρ is the desired aerosol mass concentration. The left-hand side of Eq. (5) is the quantity measured from Eq. (1); the *MAE* may be determined from Eq. (4) or from empirical measurements; and thus the aerosol mass concentration is obtained from solving Eq. (4) for the desired quantity ρ,

$$\rho = \beta_{\text{abs}}/MAE \tag{6}$$

The *MAE* for SiO_2 and kaolinite is shown in Fig. 9. The average SiO_2 absorption is obtained from

$$MAE = \frac{1}{3}MAE_{c-axis} + \frac{2}{3}MAE_{a-axis} \tag{7}$$

The factor of 2 in the second term is due to the a-axis being doubly represented as shown in Fig. 4. This model assumes

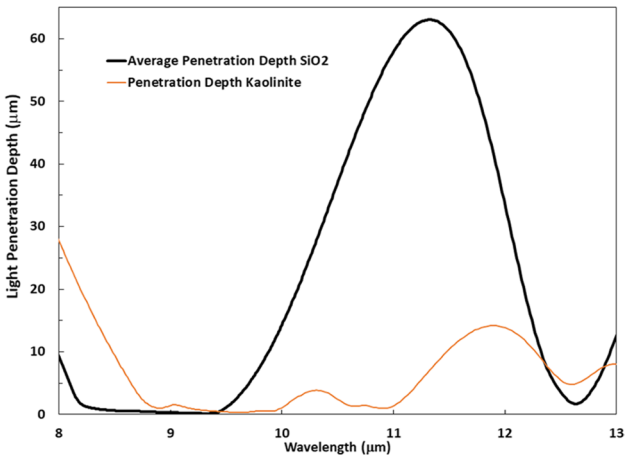

Fig. 8 Light penetration depth as a function of wavelength for SiO_2 and kaolinite

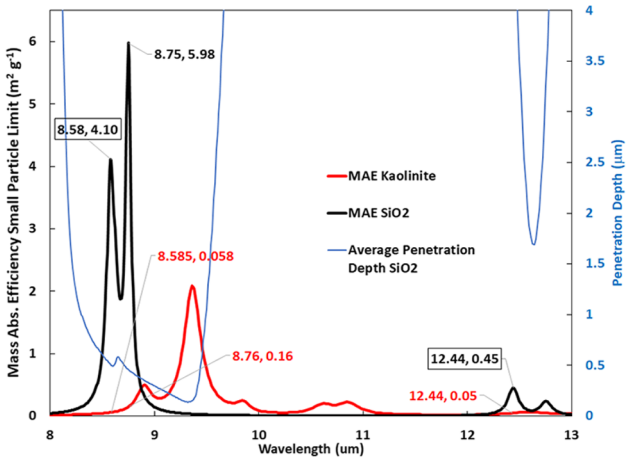

Fig. 9 Average MAE for SiO_2 and kaolinite (left axis) and the penetration depth (right axis) as a function of light wavelength. Candidate wavelengths for the laser wavelength of the photoacoustic instrument are the first number in the ordered pairs while the second number is the corresponding mass absorption efficiency

Table 1 Summary of possible wavelengths for the photoacoustic instrument measurement of SiO_2 with minimal interference from kaolinite. In comments, green is desirable, and red is not

λ (microns)	Wavenumber (cm^{-1})	*MAE* SiO_2	*MAE* Kaolinite	Comment
8.58	**1165.5**	**4.10**	**0.058**	Great kaolinite rejection; small δ
8.75	1142.9	5.98	0.16	Okay kaolinite rejection; small δ
12.44	**803.9**	**0.45**	**0.05**	Larger δ; smaller kaolinite rejection

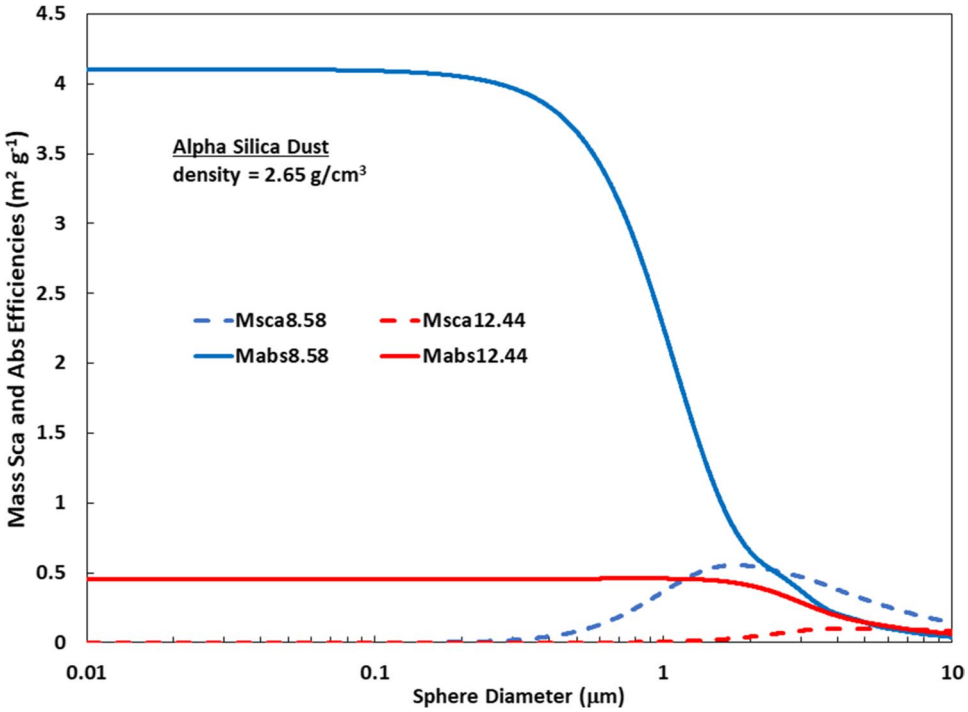

Fig. 10 Average over crystal axes orientation SiO_2 mass absorption and scattering efficiencies calculated from Mie theory as a function of aerosol diameter for 8.58 and 12.44 microns. In the legend, Msca8.58 (for example) refers to the mass scattering efficiency at 8.58 microns

that there is no preferred orientation of the SiO_2 crystalline axes relative to the polarization direction of the light.

Figure 9 gives both the *MAE* and the light penetration depth for SiO_2, along with candidate ordered pairs of values as candidate laser wavelengths (μm) and the *MAE* ($m^2\ g^{-1}$). Table 1 summarizes the choices for laser wavelength based on Fig. 10. Wavelengths are chosen where the *MAE* for SiO_2 is large. The best candidate laser wavelengths are shown in bold: $\lambda = 8.58$ microns and $\lambda = 12.44$ microns.

2.2.4 Model for the Mass Absorption and Scattering Efficiencies at the Instrument Candidate Wavelengths, Accounting for Aerosol Size

Figure 10 and Fig. 11 show the Mie theory [8] calculated mass scattering and absorption efficiencies for SiO_2 and kaolinite, respectively, at the candidate wavelengths. The flat portions of the MAE curves for SiO_2 are associated with that wavelength range where light absorption is independent of aerosol diameter, ideal for determination of the aerosol mass concentration. Figure 10 shows that the flatness

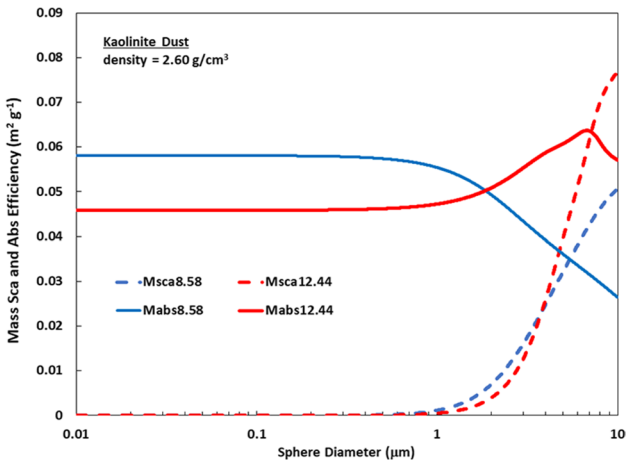

Fig. 11 Same as Fig. 10 but for kaolinite

of the mass absorption efficiency curve for a wavelength of 12.44 microns extends to an aerosol diameter of around 2 microns, whereas at 8.58 microns, it extends only to about 1

micron before steeply declining. The mass absorption efficiency for kaolinite is much smaller in comparison to SiO_2 at these wavelengths, as shown in Fig. 11. Thus, the ideal laser wavelength is 12.44 microns because it is a tradeoff between moderate to strong absorption and penetration of the laser radiation into the particle. It should be noted that respirable aerosol may include dust with diameters larger than 10 microns as well so that, depending on the aerosol mass distribution in mines, the contribution of these larger aerosol may be important.

3 Mass Absorption Efficiency for Coal, Water Vapor, and Carbon Dioxide Compared to SiO_2 and Kaolinite

Research has been done previously on the real and imaginary refractive indices for coal [23]. These data were digitized and used for computations of the optical properties of coal. Assuming a coal mass density of 1.4 g/cm^3, the small particle limit mass absorption efficiency for bituminous coal was computed and is shown in Fig. 12 along with those of SiO_2 and kaolinite. In reported previous research, coal dust was not a strong interferent for the FTIR measurements of SiO_2 [11]. The absorption coefficient for water vapor and carbon dioxide are also shown in Fig. 12 for typical ambient concentrations. Theoretical absorption spectra were computed using gas cell modeling for transmittance within spectralcalc.com and converting this to absorption for the gas concentrations given in the caption of Fig. 12. Notice that there are several peaks in H_2O's mass absorption efficiency located right around the peaks related to SiO_2. These peaks represent strong interference by H_2O. Special care must be taken to choose a wavelength for SiO_2 quantification that does not include one of these peaks. However, the presence of these peaks has an advantage. If the photoacoustic instrument has a relative humidity and air temperature sensor built into it, it can quantify the water vapor concentration. With this value known, a wavelength can be chosen to measure the absorption coefficient, β_{abs}, of water vapor. Because this allows for correlation between the water vapor's measured absorption coefficient and calculated concentration, this information can be used to calibrate the photoacoustic instrument's SiO_2 concentration calculation. Photoacoustic instruments typically have a measurement cycle consisting of a particle free background determination that responds to gaseous light absorption followed by a foreground measurement that responds to gaseous and aerosol light absorption [12]. Aerosol light absorption is obtained by the difference of foreground and background measurements.

4 Effect of Acoustic Resonant Frequency and Photoacoustic Response

The choice of acoustic resonator frequency is related to resonator geometry and size. It is important for

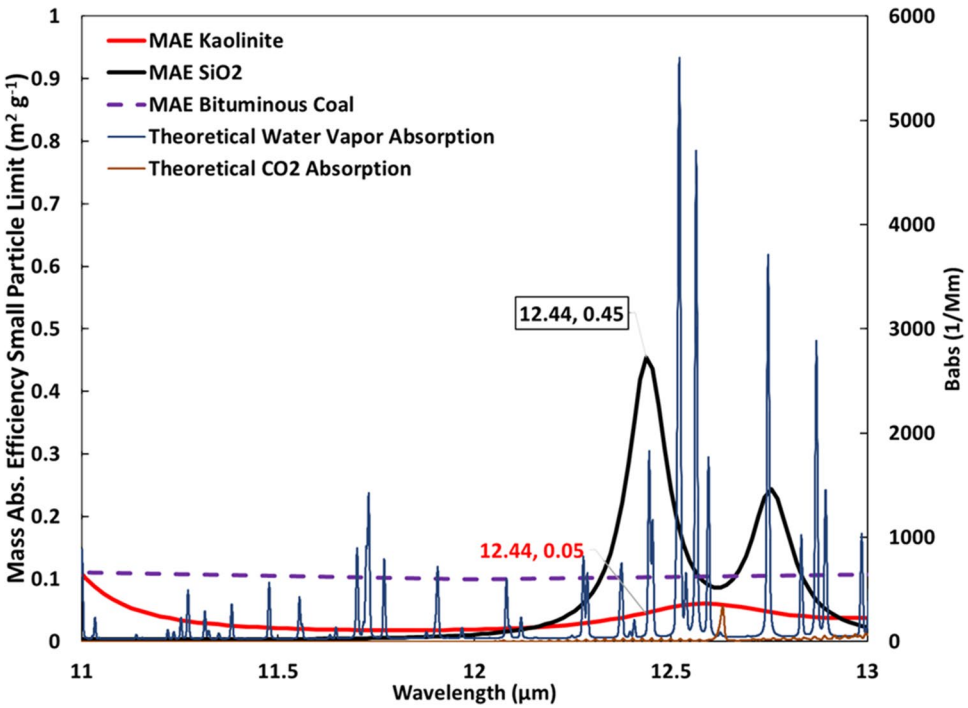

Fig. 12 Small particle limit of the mass absorption efficiency for SiO_2 (black curve), kaolinite (red curve), and bituminous coal. Also includes absorption coefficient for water vapor and carbon dioxide. Water vapor and carbon dioxide mixing ratios of 6.83 g/kg and 408 ppm, respectively, at a temperature of 296 K and pressure of 86,100 Pa representative of Reno NV ambient conditions. The water vapor concentration corresponds to a relative humidity of 33%. The ordered pairs are as discussed in Fig. 9

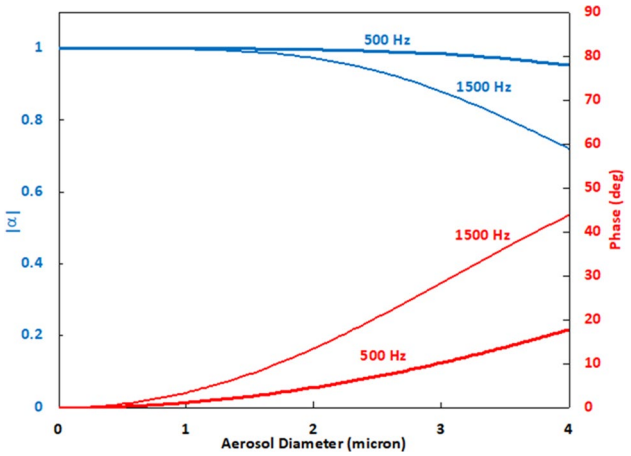

Fig. 13 Amplitude and (left y-axis) and phase (right y-axis) of the modeled photoacoustic signal response for RCS as a function of aerosol diameter at two acoustical frequencies. A 500-Hz operation has a flatter (and thus better) amplitude and phase response because heat can come out of the aerosol during laser beam modulation at the lower frequency

quantitative measurements of light absorption. This is because laser heated aerosols have a finite time for that heat to transfer to the surrounding air between laser pulses [8]. The response time τ for heat to diffuse from an aerosol of radius r to the surrounding air having thermal conductivity κ_{air} is:

$$\tau = \frac{r^2 \rho_{\mathrm{RCS}} c_{\mathrm{RCS}}}{3\kappa_{\mathrm{air}}} \tag{8}$$

where ρ_{RCS} and c_{RCS} are the density and heat capacity per unit mass of RCS [8]. The response of the photoacoustic signal at a frequency f as affected by heat transfer time is [8]:

$$\alpha = \frac{1}{1 - i2\pi f\tau} \tag{9}$$

where i is the unit imaginary number. Figure 13 shows the amplitude and phase response of laser heated RCS aerosol as a function of aerosol diameter. The left y-axis shows the relative amplitude of the aerosol light absorption signal and ideally would have a value of unity for all aerosol diameters. A 500-Hz operation is closer to ideal than is 1500 Hz. The phase shift is usually measured with photoacoustic instruments and can indicate the presence of larger aerosol when it is greater than zero. It may provide a correction for the reduced photoacoustic response for larger particles at 1500 Hz.

Recent research has demonstrated the utility of a miniature Helmholtz resonator–based photoacoustic instrument for methane detection using a quantum cascade laser at 3.36-microns wavelength [24]. The instrument used was approximately 3″ long, though operated at 2000 Hz, which is rather high for silica detection because of the higher response time. However, their research establishes the utility of Helmholtz resonator detectors so that a compact 500-Hz device may be developed for RCS detection. A lower frequency instrument is desirable for dust measurements in order to mitigate phase-lag. Additionally, aerosol detection is more challenging than trace gas detection because special precautions must be employed to manage the eventual dirtying of the resonator windows by aerosol deposition.

5 Recommendations for Photoacoustic RCS Measurements

Figure 12 suggests that RCS has a strong absorption feature at 12.44 microns, with possibly some interference by kaolinite and coal dust to be expected. Kaolinite has relatively strong absorption at 11 microns with some coal dust interference, though negligible RCS interference. Coal dust is the dominant absorber at 12 microns. A tunable quantum cascade laser photoacoustic instrument operating in this spectral range can thus be used to determine the concentration of RCS and correct for interference by coal and kaolinite dust. Absorption by water vapor can be used to check the instrument calibration. Carbon dioxide gas does not interfere with measurements in this range. Additionally, it is desired to have a photoacoustic instrument operating at a frequency of around 500 Hz so that aerosol thermal response time does not introduce aerosol size-dependent response to the instrument as shown in Fig. 13. Finally, the complex mineralogy of non-coal mines would need to be addressed for determination of RCS in them.

Funding This study was funded by the National Institute for Occupational Safety and Health under project number HCCR-2019–35129.

Data Availability Spectral calc absorption data for water vapor and CO_2: https://www.spectralcalc.com/info/about.php

Code Availability Absorption by small particles: https://www.astro.princeton.edu/~draine/scattering.html

Declarations

Ethics Approval This study does not involve human or animal subjects.

Competing Interests The authors declare no competing interests.

References

1. MSHA (2010) Coal mine dust sampling devices; high-voltage continuous mining machine standard for underground coal mines; Final Rules, 75 FR 17511. Mine Safety and Health Administration
2. Vincent JH (2005) Health-related aerosol measurement: a review of existing sampling criteria and proposals for new ones. J Environ Monit 7:1037–1053
3. MSHA (2014) Lowering miners' exposure to respirable coal mine dust, including continuous personal dust monitors; Final Rule, 79 FR 24813. Mine Safety and Health Administration
4. NIOSH (2011) Current Intelligence Bulletin 64: coal mine dust exposures and associated health outcomes. National Institute for Occupational Safety and Health, pp 1–31
5. Reynolds K, Jerome J: Silicosis. vol. 69. pp. 51: Sage Publishing; 2021:51.
6. Hart JF, Autenrieth DA, Cauda E, Chubb L, Spear TM, Wock S, Rosenthal S (2018) A comparison of respirable crystalline silica concentration measurements using a direct-on-filter Fourier transform infrared (FT-IR) transmission method vs a traditional laboratory X-ray diffraction method. J Occupational Environ Hygiene 15:743–754
7. Pampena JD, Cauda EG, Chubb LG, Meadows JJ (2020) Use of the field-based silica monitoring technique in a coal mine: a case study. Mining Metallurgy & Exploration 37:717–726
8. Moosmuller H, Chakrabarty RK, Arnott WP (2009) Aerosol light absorption and its measurement: a review. J Quant Spectrosc Radiat Transfer 110:844–878
9. Lewis K, Arnott WP, Moosmuller H, Wold CE (2008) Strong spectral variation of biomass smoke light absorption and single scattering albedo observed with a novel dual-wavelength photoacoustic instrument. J Gerontol Ser A Biol Med Sci 113:14
10. Gyawali M, Arnott WP, Zaveri RA, Song C, Moosmuller H, Liu L, Mishchenko MI, Chen LWA, Green MC, Watson JG, Chow JC (2012) Photoacoustic optical properties at UV, VIS, and near IR wavelengths for laboratory generated and winter time ambient urban aerosols. Atmos Chem Phys 12:2587–2601
11. Miller AL, Weakley AT, Griffiths PR, Cauda EG, Bayman S (2017) Direct-on-filter alpha-quartz estimation in respirable coal mine dust using transmission Fourier transform infrared spectrometry and partial least squares regression. Appl Spectrosc 71:1014–1024
12. Kocsis C, Arnott WP, Witherspoon A, Tesfasion S (2019) Development of an advanced real-time personal coal dust monitoring instrument based on photo-acoustic spectroscopy. Alpha Foundation, pp 1–49. https://www.alpha-foundation.org/hsi/afc518-54_utah_finalrpt/
13. Wei SJ, Kulkarni P, Ashley K, Zheng LN (2017) Measurement of crystalline silica aerosol using quantum cascade laser-based infrared spectroscopy. Sci Rep 7:8
14. Arnott WP, Moosmuller H, Rogers CF, Jin TF, Bruch R (1999) Photoacoustic spectrometer for measuring light absorption by aerosol: instrument description. Atmos Environ 33:2845–2852
15. Arnott WP, Moosmuller H, Walker JW (2000) Nitrogen dioxide and kerosene-flame soot calibration of photoacoustic instruments for measurement of light absorption by aerosols. Rev Sci Instrum 71:4545–4552
16. Arnott WP, Hamasha K, Moosmuller H, Sheridan PJ, Ogren JA (2005) Towards aerosol light-absorption measurements with a 7-wavelength aethalometer: evaluation with a photoacoustic instrument and 3-wavelength nephelometer. Aerosol Sci Technol 39:17–29
17. Adams KM (1988) Real-time in situ measurements of atmospheric optical-absorption in the visible via photoacoustic-spectroscopy 1. Eval Photoacoustic Cells Appl Optics 27:4052–4056
18. Fujita EM, Zielinska B, Campbell DE, Arnott WP, Sagebiel JC, Mazzoleni L, Chow JC, Gabele PA, Crews W, Snow R et al (2007) Variations in speciated emissions from spark-ignition and compression-ignition motor vehicles in California's south coast air basin. J Air Waste Manag Assoc 57:705–720
19. Arnott WP, Walker JW, Moosmuller H, Elleman RA, Jonsson HH, Buzorius G, Conant WC, Flagan RC, Seinfeld JH (2006) Photoacoustic insight for aerosol light absorption aloft from meteorological aircraft and comparison with particle soot absorption photometer measurements: DOE Southern Great Plains climate research facility and the coastal stratocumulus imposed perturbation experiments. J Geophys Res Atmos 111:D05S02
20. Di Biagio C, Boucher H, Caquineau S, Chevaillier S, Cuesta J, Formenti P (2014) Variability of the infrared complex refractive index of African mineral dust: experimental estimation and implications for radiative transfer and satellite remote sensing. Atmos Chem Phys 14:11093–11116
21. Zeidler S, Posch T, Mutschke H (2013) Optical constants of refractory oxides at high temperatures mid-infrared properties of corundum, spinel, and alpha-quartz, potential carriers of the 13 mu m feature. Astron Astrophys 553:15
22. Glotch TD, Rossman GR, Aharonson O (2007) Mid-infrared (5–100 micron) reflectance spectra and optical constants of ten phyllosilicate minerals. Icarus 192:605–622
23. Foster PJ, Howarth CR (1968) Optical constants of carbons and coals in infrared. Carbon 6:719–0
24. Rouxel J, Coutard J-G, Gidon S, Lartigue O, Nicoletti S, Parvitte B, Vallon R, Zeninari V, Gliere A (2016) Miniaturized differential Helmholtz resonators for photoacoustic trace gas detection. Sensors and Actuators B-Chemical 236:1104–1110